Applied Physics Letters

RESEARCH ARTICLE | MARCH 25 2025

Enhancing the circular photogalvanic effect in double Weyl semimetals via symmetry breaking

Tongshuai Zhu ; Hao Ni ; Dinghui Wang ; Zhilong Yang ; Guohui Zhan ; Baojun Wei

Appl. Phys. Lett. 126, 123103 (2025)
https://doi.org/10.1063/5.0257016

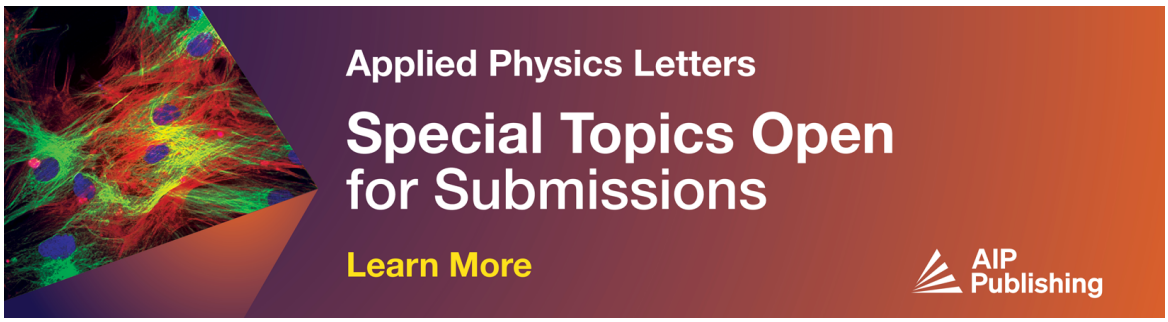

Applied Physics Letters ARTICLE pubs.aip.org/aip/apl

Enhancing the circular photogalvanic effect in double Weyl semimetals via symmetry breaking

Cite as: Appl. Phys. Lett. **126**, 123103 (2025); doi: 10.1063/5.0257016
Submitted: 8 January 2025 · Accepted: 28 February 2025 ·
Published Online: 25 March 2025

Tongshuai Zhu,[1,2] Hao Ni,[1] Dinghui Wang,[3,a)] Zhilong Yang,[4,a)] Guohui Zhan,[5,a)] and Baojun Wei[1]

AFFILIATIONS

[1]College of Science, China University of Petroleum (East China), Qingdao 266580, China
[2]School of Materials Science and Engineering, China University of Petroleum (East China), Qingdao 266580, China
[3]School of Materials Science and Physics, China University of Mining and Technology, Xuzhou 221116, China
[4]Beijing National Laboratory for Condensed Matter Physics, and Institute of Physics, Chinese Academy of Sciences, Beijing 100190, China
[5]School of Physics, Zhejiang University, Hangzhou 310058, China

[a)]**Authors to whom correspondence should be addressed:** wangdh@cumt.edu.cn; zhlyang@iphy.ac.cn; and ghzhan@zju.edu.cn

ABSTRACT

Weyl semimetals have emerged as a hot topic in condensed matter physics in last decade. Beyond their intriguing electrical transport phenomena, such as the negative magnetoresistance driven by the chiral anomaly and the anomalous Hall effect, they also exhibit intriguing second-order optoelectronic responses, such as the circular photogalvanic effect (CPGE). In this Letter, we investigate the CPGE in a class of double Weyl semimetal protected by the $C_{3z}\mathscr{T}$ symmetry by using the effective model. Unlike double Weyl semimetal protected by C_{nz} (n = 4, 6) symmetry, when time-reversal symmetry $\mathscr{T}$ is broken, one $C_{3z}\mathscr{T}$-protected double Weyl point (WP) evolves into four single WPs, three of which are related by C_{3z} symmetry, and these WPs share the same topological charge and reside at the same energy level. This unique configuration enhances the CPGE trace due to the combined topological charge of the three WPs, resulting in a higher quantized plateau. Our findings provide promising prospects for the development of optoelectronic devices in the future.

Topological semimetals have emerged as an intriguing class of quantum materials over the past decades, characterized by robust nodal points or lines in momentum space, such as Dirac semimetals,[1–3] Weyl semimetals,[4–7] and nodal-line semimetals.[8–10] Among them, Weyl semimetals have garnered a significant attention due to the presence of low-energy excitations known as Weyl fermions. Weyl semimetals are characterized by linear band crossings and Fermi arc surface states. In solid, the protection of lattice symmetries allows the Weyl points (WPs) to exhibit not only linear dispersions but also quadratic or even exhibit higher-order dispersions.[11–16] WPs with linear dispersions along all directions and a monopole charge of $|\chi| = 1$ are referred to as single WPs, which have been extensively studied in materials such as TaAs family.[17–20] When WPs exhibit higher-order band dispersions, they can carry larger monopole charges. For instance, double WPs, characterized by quadratic dispersion in the plane and a monopole charge of $|\chi| = 2$, can be discovered in materials such as $HgCr_2Se_4$,[16,21] $SrSi_2$,[22] and $BaNiIO_6$.[23]

Weyl semimetals host intriguing transport phenomena, including negative magnetoresistance related to the chiral anomaly[24–27] and the quantum anomalous Hall effect.[28,29] In addition to electronic transport phenomena, they also exhibit a variety of nonlinear optical responses,[30–39] such as the circular photogalvanic effect (CPGE), a photocurrent induced by circularly polarized light (CPL) at the second order of the electric field. Remarkably, the CPGE trace can be quantized to the monopole charge of the WPs at specific optical frequencies.[40–51]

For a double WP with a monopole charge of $\chi = 2$, its CPGE trace quantizes to $2i\beta_0$, where $\beta_0 = \frac{\pi e^3}{h^2}$. If the symmetry protecting the double WP is broken, causing it to split into single WPs, the CPGE trace is generally expected to quantize to $i\beta_0$ or $2i\beta_0$ at most, without further enhancement. This assumption relies on the scenario where the double WP splits into two single WPs with identical monopole charges. Are there other possible scenarios for the evolution of a double WP into single WPs? To address this question, we first

analyze the double WP from the perspective of symmetry. The double Weyl semimetal can be protected by rotational symmetries such as C_{nz} ($n = 4, 6$), or by the combination of threefold symmetry C_{3z} and time-reversal symmetry $\mathscr{T}$ when the spin–orbit coupling (SOC) is neglected.[11] For a double WP protected by the rotational symmetry, breaking the corresponding symmetry typically results in the double WP splitting into two single WPs. In contrast, for a double WP protected by $C_{3z}\mathscr{T}$, breaking time-reversal symmetry $\mathscr{T}$ while preserving C_{3z} ensures that the resulting single WPs remain related by C_{3z}. Moreover, the no-go theorem[52,53] mandates that the total monopole charge is conserved, allowing for scenarios such as three single WP with $\chi = 1$ and a single WP with $\chi = -1$, as illustrated in Fig. 1(a). Notably, the three single WPs with $\chi = 1$ reside at the same energy level, potentially leading to an enhancement in the CPGE trace.

In this Letter, we calculate the CPGE trace for a double WP protected by $C_{3z}\mathscr{T}$ symmetry using an effective $k \cdot p$ model. Our results show that when $\mathscr{T}$ is broken while preserving C_{3z} symmetry, a double WP with monopole charge of $\chi = 2$ splits into three single WPs with a topological charge of $\chi = 1$ and one single WP with a topological charge of $\chi = -1$. The three single WPs with a topological charge of $\chi = 1$ are related by C_{3z} symmetry and consistently reside at the same energy level. When the Fermi level tuned near these three single WPs, an enhancement in CPGE is observed within a specific frequency range, and the CPGE can quantize to $3i\beta_0$. Additionally, we identify a visual criterion within the two-band model to determine whether the CPGE can be quantized. This criterion involves examining the relationship between the Fermi surface and the isosurfaces of the energy difference between the conduction and valence bands at a given optical frequency. Finally, we discuss the practical approaches for realizing the CPGE enhancement, which can be achieved through driving by laser or external magnetic fields.

We begin from a $\boldsymbol{k} \cdot \boldsymbol{p}$ Hamiltonian within the irreducible representations Γ_3 of the space group 149, which is written as[54,55]

$$H_{\mathrm{DW}} = \varepsilon_{\boldsymbol{k}} + vk_z\sigma_z + (t_1 k_z k_- - t_2 k_+^2)\sigma_+ + \mathrm{H.c.}, \tag{1}$$

where $\varepsilon_{\boldsymbol{k}} = \varepsilon_0 + a(k_x^2 + k_y^2) + bk_z^2$, $k_\pm = k_x \pm k_y$, and $\sigma_\pm = (\sigma_x \pm \mathrm{i}\sigma_y)/2$ with σ_i $(i = x, y, z)$ represent the Pauli matrices. The Hamiltonian exhibits a double WP protected by $C_{3z}\mathscr{T}$ symmetry. The matrix representations of the time-reversal operator and the threefold rotational operator are given by $\hat{\mathscr{T}} = -i\sigma_x\hat{\mathscr{K}}$ and $\hat{C}_{3z} = \mathrm{diag}\left(e^{i\frac{2\pi}{3}}, e^{-i\frac{2\pi}{3}}\right)$, respectively. Notably, when $a = 0$, the above-mentioned Hamiltonian can also describe a double WP protected by rotational symmetry. Weyl semimetals exhibit intriguing optical responses. One such phenomenon is the CPGE injection current, which refers to the second-order optical response induced by CPL. The CPGE injection current is defined as

$$\frac{dJ_i}{dt} = \beta_{ij}(\omega)[\boldsymbol{E}(\omega) \times \boldsymbol{E}^*(\omega)]_j, \tag{2}$$

where $\boldsymbol{E}(\omega)$ represents the electric field of the CPL, ω is the optical frequency of the CPL, and β_{ij} is the CPGE tensor. The CPGE tensor for the two band model is given by[40]

$$\beta_{ij}(\omega) = \frac{i\pi e^3}{\hbar^2 V}\sum_{\boldsymbol{k}} \Delta f_{\boldsymbol{k},12}\partial_{k_i}E_{\boldsymbol{k},12}\Omega^j_{\boldsymbol{k}}\delta(\hbar\omega - E_{\boldsymbol{k},21}), \tag{3}$$

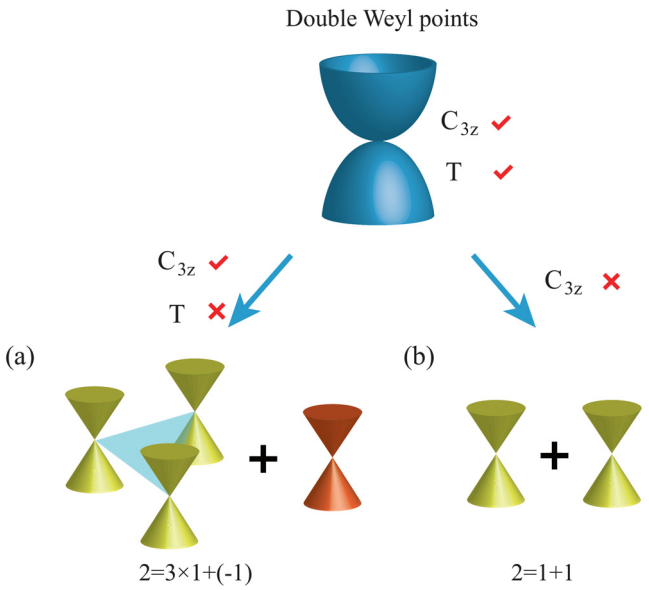

FIG. 1. A schematic diagram depicting two scenarios in which a $C_{3z}\mathscr{T}$-protected double Weyl point (WP) evolves into single WPs under different symmetry-breaking conditions. (a) When the C_{3z} symmetry is preserved but the time-reversal symmetry $\mathscr{T}$ is broken, a double WP with a monopole charge of $\chi = 2$ splits into three single WPs with a monopole charge of $\chi = 1$ and one SWP with a monopole charge of $\chi = -1$. (b) When the C_{3z} symmetry is broken, a double WP with a monopole charge of $\chi = 2$ splits into two single WPs, each with a monopole charge of $\chi = 1$. The expressions "$2 = 3 \times 1 + (-1)$" and "$2 = 1 + 1$" represent the conversion relationships of WPs in these two scenarios.

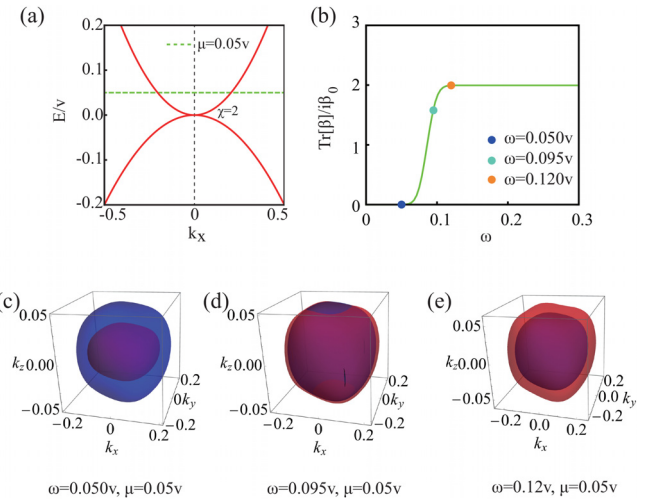

FIG. 2. The quantized CPGE trace for a double WP protected by $C_{3z}\mathscr{T}$ symmetry. (a) The in-plane band structures of the double WP. (b) The CPGE trace as a function of photon frequency at the Fermi level $\mu = 0.05v$. (c)–(e) The three-dimensional Fermi surface (S_1, blue surfaces) at $\mu = 0.05v$ and the isosurfaces of $E_{\boldsymbol{k},21}$ (S_2, red surfaces) at $\omega = 0.05v$ (c), $\omega = 0.095v$ (d), and $\omega = 0.12v$ (e). The parameters are $\varepsilon_0 = 0$, $a = b = 0.2v$, and $t_1 = t_2 = v$.

where V is the sample volume, $\Delta f_{\boldsymbol{k},12} = f_{\boldsymbol{k},1} - f_{\boldsymbol{k},2}$, $f_{\boldsymbol{k},1,2}$ are Fermi–Dirac distributions of the valence (1) and conduction (2) bands, $E_{\boldsymbol{k},12} = E_{\boldsymbol{k},1} - E_{\boldsymbol{k},2}$ represents the energy difference between the bands, and $\Omega^j_{\boldsymbol{k}}$ is the Berry curvature.

We first calculate the trace of the CPGE for a double WP. As shown in Fig. 2(a), the double WP exhibits a quadratic dispersion in the plane. According to Eq. (3), if we plot the Fermi surface, only the points outside the Fermi surface are singly occupied (here we only study the type-I WP), we label the Fermi surface as S_1. The delta function accounts for the optical selection rule and selects a surface enclosing the WP, which we label as S_2. The term $\Delta f_{\boldsymbol{k},12}$ selects the states only occupied by the valence band. If S_2 is entirely enclosed by S_1, as illustrated in Fig. 2(c) at $\omega = 0.05v$, there are no singly occupied states inside the Fermi surface, resulting in a strictly zero CPGE trace. Conversely, if S_1 is completely enclosed by S_2, as depicted in Fig. 2(e) at $\omega = 0.12v$, the CPGE trace corresponds to the integral of the Berry flux over the surface S_2. In this case, the CPGE trace is quantized and equals the monopole charge of the WPs inside the surface S_2. If S_2 intersects with S_1, as shown in Fig. 2(d) at $\omega = 0.095v$, or if S_2 fails to form a closed surface, the CPGE trace is not quantized.

When considering the symmetry-breaking term $m_x\sigma_x$, both the C_{3z} symmetry and time-reversal symmetry $\mathscr{T}$ are broken, causing the double WP to split into two single WPs with monopole charge of $\chi = 1$, located at $\left(\pm\sqrt{\frac{m}{t_1}}, 0, 0\right)$ as shown in Fig. 1(b). In this case, the CPGE trace cannot be enhanced. When the $\mathscr{T}$-breaking term $m_z\sigma_z$ is introduced, the double WP splits into three single WPs with monopole charge $\chi = 1$ located at $\left(-\frac{m_z w}{vb}, 0, -\frac{m_z}{v}\right)$, $\left(\frac{m_z w}{2vb}, \pm\frac{\sqrt{3}m_z w}{2vb}, -\frac{m_z}{v}\right)$ and one single WP with topological charge $\chi = -1$ located at $\left(0, 0, -\frac{m_z}{v}\right)$. The three single WPs with monopole charge $\chi = 1$ are related by C_{3z}, and thus, they will always lie at the same Fermi level. For the transport properties associated with the WPs, these three single WPs contribute simultaneously. In Fig. 3(a), we plot the energy bands along the paths of the two split SWPs from the Γ point, where C_1 carries a topological charge of $\chi = -1$ and C_2 carries a topological charge of $\chi = 1$. In Fig. 3(b), we calculated the variation of the CPGE trace with optical frequency for different Fermi levels. When the fermi energy is close to C_1, such as the blue lines ($\mu = 0.03v$) in Fig. 3(b), at low optical frequencies, the CPGE trace is negative. As the frequency increases, it transitions to positive values, demonstrating the potential to reverse the direction of the photocurrent. When the fermi level is set at $\mu = 0.12v$ (green lines), which is close to C_2, as the optical frequency gradually increases from 0, the CPGE trace increases, reaching a maximum of nearly $3i\,\beta_0$ around $\omega = 0.1v$. As ω continues to increase, the CPGE trace gradually decreases and quantizes to $2i\,\beta_0$. Compared with the case when $C_{3z}\mathscr{T}$ is preserved, the CPGE trace shows a significant increase at certain optical frequencies. The enhancement of the CPGE trace originates from the splitting of the double WP into three single WPs with the same topological charge, connected by the C_{3z} symmetry. In Figs. 3(c) and 3(d), we illustrate the Fermi surface (blue) at $\mu = 0.12v$ alongside the isosurface of $E_{\boldsymbol{k},21}$ (red) for $\omega = 0.11v$ and $\omega = 0.22v$, respectively. The Fermi surface forms four closed surfaces, each enclosing one WP. When $\omega = 0.22v$, the isosurface of $E_{\boldsymbol{k},21}$ completely encloses the Fermi surface. At this point, the CPGE trace equals the sum of the topological charges of all the WPs inside the isosurface, resulting in the CPGE trace being quantized to $2i\,\beta_0$. When $\omega = 0.12v$, the isosurface forms four closed surfaces around each WP. At this point, only the isosurface around the WPs with $\chi = 1$ completely encloses the Fermi surface, while the isosurface near the WPs with $\chi = -1$ lies inside the Fermi surface. According to our earlier discussion, only the WPs with $\chi = 1$ contribute to the CPGE trace at this stage, resulting in the CPGE trace being quantized to $3i\,\beta_0$.

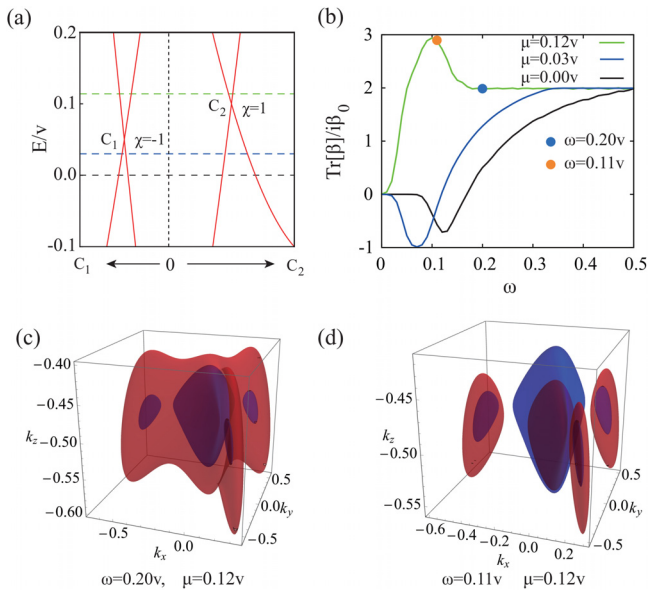

FIG. 3. The CPGE trace for the Hamiltonian Eq. (1) with a $\mathscr{T}$-breaking term $m_z\sigma_z$. (a) The band structures along the two Weyl points (WPs). (b) The CPGE trace as a function of photon frequency at different Fermi levels. (c) and (d) The three-dimensional Fermi surface (S1, blue surface) at $\mu = 0.12v$ and the isosurfaces of $E_{\boldsymbol{k},21}$ (S2, red surfaces) at $\omega = 0.2v$ (c) and $\omega = 0.12v$ (d). The parameters are $\varepsilon_0 = 0$, $a = b = 0.2v$, $t_1 = t_2 = v$, and $m_z = 0.5v$.

The preceding discussion focuses on the behavior of one doble WP. To better approximate a realistic system, we consider the following tight-binding Hamiltonian:

$$
\begin{aligned}
H_{TB} = &\left[2a(1-\cos k_z) - \frac{4}{3}b\left(\cos k_y + 2\cos\frac{\sqrt{3}k_x}{2}\cos\frac{k_y}{2}\right)\right.\\
&\left.+\frac{8}{3}w\left(2\cos\frac{\sqrt{3}k_x}{2}\sin\frac{k_y}{2} - \sin k_y\right)\right]\sigma_0\\
&+\frac{1}{3}\left(8\sqrt{3}t_1\sin\frac{\sqrt{3}k_x}{2}\sin\frac{k_y}{2} + 3t_2\sin k_y\sin k_z\right)\sigma_y\\
&+\left[\frac{8}{3}t_1\left(\cos\frac{\sqrt{3}k_x}{2}\cos\frac{k_y}{2} - \cos k_y\right)\right.\\
&\left.+\frac{2t_2\cos\frac{k_y}{2}\sin\frac{\sqrt{3}k_x}{2}\sin k_z}{\sqrt{3}}\right]\sigma_x + (m_z + v\sin k_z)\sigma_z. \qquad (4)
\end{aligned}
$$

The Hamiltonian is regularized from the continuum model in Eq. (1) onto a three-dimensional hexagonal lattice, where the lattice constants are defined as $\boldsymbol{a}_1 = (\frac{\sqrt{3}}{2}, \frac{1}{2}, 0)^T$, $\boldsymbol{a}_2 = (\frac{\sqrt{3}}{2}, -\frac{1}{2}, 0)^T$, and $\boldsymbol{a}_3 = (0, 0, 1)^T$. The representation matrix of the symmetry operator

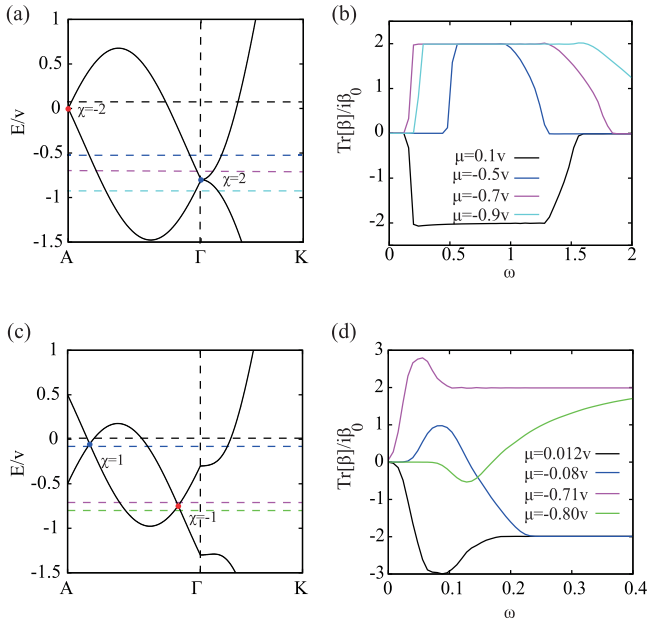

FIG. 4. The calculated CPGE trace for the tight-binding model in Eq. (4). (a) and (c) The band structure for $m_z = 0$ (a) and $m_z = 0.5$ (c). (b) and (d) The CPGE trace with different Fermi levels for $m_z = 0$ (b) and $m_z = 0.5v$ (d). The parameters are $a = b = 0.2v$ and $t_1 = t_2 = w = v$.

is the same as that in the continuum model, in which the time-reversal operator and the threefold rotational operator are written as $\hat{\mathscr{T}} = -i\sigma_x\hat{\mathscr{K}}$ and $\hat{C}_{3z} = \mathrm{diag}\left(e^{i\frac{2\pi}{3}}, e^{-i\frac{2\pi}{3}}\right)$. The band structures without $\mathscr{T}$-breaking are shown in Fig. 4(a). In this case, a pair of double WPs with monopole charges of $\chi = 2$ and $\chi = -2$ are located at Γ and A, respectively. When the Fermi surface is near the double WP with a monopole charge of $\chi = 2$, the CPGE trace becomes quantized to $2i\beta_0$ over a specific frequency range. As the Fermi level approaches the WP, the range of optical frequencies where the CPGE trace is quantized broadens. From the discussion of the continuum model, whether the CPGE trace is quantized depends on whether the isosurface of $E_{\boldsymbol{k},21}$ forms a closed surface and its relationship with the Fermi surface. When $m_z \neq 0$, the time-reversal symmetry is broken and the threefold rotational symmetry is preserved. While considering a symmetry breaking term $m_x\sigma_x$ or $m_y\sigma_y$, both the time-reversal symmetry and the threefold rotational symmetry are broken. In the following, we focus on the case that $m_z \neq 0$ in which the threefold rotational symmetry is preserved. As shown in Fig. 4(c), the original double WPs at Γ and A split into four pairs of single WPs, one of which remains on the k_z-axis. The monopole charge of the single WPs on the k_z-axis has opposite signs compared to the original double WPs. In Fig. 4(d), the CPGE trace is calculated for different Fermi levels. When the Fermi energy is near the three C_{3z}-related single WPs originating from the double WP at the Γ point ($\mu = -0.71v$), as the optical frequency increases, the CPGE trace (purple lines) initially increases to nearly $3i\beta_0$ and then decreases to be quantized to $2i\beta_0$. On the other hand, when the Fermi level is near the single WP on the k_z-axis ($\mu = -0.80v$), the CPGE trace (green lines) first decreases, then undergoes a sign reversal, and eventually quantizes to $2i\beta_0$. For the three C_{3z}-related single WPs originating from the double WP at A, the CPGE trace initially decreases to nearly $-3i\beta_0$ and then gradually increases to be quantized to $-2i\beta_0$. When the Fermi level is near the SWP on the k_z-axis originating from the double WP at A, the CPGE trace first increases to nearly $i\beta_0$ and then decreases to be at $-2i\beta_0$. At sufficiently high optical frequencies, the CPGE trace aligns with the results for the case without symmetry breaking. However, at low optical frequency, the CPGE trace exhibits two distinct behaviors: when the Fermi level is near the three single WPs related by C_{3z} with the same monopole charge, the CPGE trace significantly increases and can quantize to $\pm 3i\beta_0$. In contrast, when the Fermi level is near the single WP at the k_z-axis, the CPGE trace undergoes a sign reversal, indicating the emergence of a photocurrent in the opposite direction.

For a realistic material, $BaNiIO_6$ may provide a promising platform to observe the CPGE enhancement. $BaNiIO_6$ is expected to crystallize in space group 149. When the SOC is neglected, the spin-up and spin-down channels in the ferromagnetic phase of $BaNiIO_6$ are decoupled, and the bands for each spin can be treated within a spinless framework. We performed the first-principles calculations for $BaNiIO_6$ by employing the Vienna *ab initio* simulation package (VASP).[56,57] The calculations employed the generalized gradient approximation (GGA) with the Perdew–Burke–Ernzerhof (PBE)[58,59] type exchange-correlation potential, and the calculated band structures and calculations details can be found in the supplementary material. In the spin-up channel, $BaNiIO_6$ is expected to host a single pair of double WPs which is protected by $C_{3z}\mathscr{T}$ near the Fermi level.[23] The double in $BaNiIO_6$ can lead to significant enhancements in various transport properties, such as the enhancement of thermoelectric performance.[60] The effective Hamiltonian at Γ can be derived as in Eq. (1), and the parameters fitted from the first-principles calculations can be found in the supplementary material. When considering the SOC, the magnetic ground state of $BaNiIO_6$ becomes ferromagnetic along the [101] direction. However, the in-plane ferromagnetic order breaks the C_{3z} symmetry. To preserve the C_{3z} symmetry, we consider SOC and a magnetic ordering along the [001] direction, and the effective Hamiltonian at Γ within the irreducible corepresentations $\{\bar{\Gamma}_5, \bar{\Gamma}_6\}$ of the magnetic space group 149.23 is derived as

$$\begin{aligned} H_{FM_{[001]}} &= H_{DW} + \Delta H, \\ \Delta H &= k_z\sigma_0 + \left[m + v_1(k_x^2 + k_y^2) + v_2k_z^2\right]\sigma_z \\ &\quad + ck_+\sigma_+ + H.c. \end{aligned} \tag{5}$$

It is also possible to generate three single WPs with the same monopole charge and one single WP with opposite monopole charge from the double WP (see the supplementary material for the expressions detailing the locations of these WPs). In $BaNiIO_6$, the SOC is relatively weak. Consequently, the transport properties appear to be predominantly influenced by the double WP. By applying an external magnetic field in the z-direction, the magnetic ground state can be switched to $FM_{[001]}$. Furthermore, as the magnetic field increases, the effective Zeeman field is also enhanced, leading to an energy-level distinction between the single WPs with topological charges of $\chi + 1$ and $\chi = -1$ originating from the double WP. Under an appropriate magnetic field, an enhancement of CPGE can be observed within a specific range of optical frequencies. The application of an external magnetic field can enhance photocurrent generation, thereby improving photodetection sensitivity. In addition to an external magnetic field, in our previous

work,[61] we demonstrated that an incident laser along the z-direction can also break $\mathscr{T}$ while preserving C_{3z} symmetry, leading to the double WP split into three single WPs with the same monopole charge and one single WP with opposite monopole charge. The use of a laser can be utilized to design ultrafast optical switches.

In summary, utilizing the effective model, we find that in a class of double WPs protected by $C_{3z}\mathscr{T}$, the CPGE can be significantly enhanced, and the photocurrent can be reversed by breaking $\mathscr{T}$ with an external magnetic field or a laser. The double WPs split into single WPs when $\mathscr{T}$ is broken, while C_{3z} symmetry still remains and constrains the number of single WPs. This allows three single WPs with the same topological charge to appear at the same energy, which not only enhances the CPGE but also other Berry phase-related transport phenomena. Our study has potential applications in the design of future electronic or optoelectronic devices.

See the supplementary material for additional information on the expression for the band dispersions of the effective model, the calculated band structures from first-principles calculations, and calculation details.

This work is supported by the Postdoctoral Fellowship Program of CPSF (Grant No. GZC20242012), the Shandong Provincial Natural Science Foundation (Grant No. ZR2024QA095), the Natural Science Foundation of China (Grant No. 12074434), and the Fundamental Research Funds for the central Universities (Grant No. 23CX06063A).

AUTHOR DECLARATIONS

Conflict of Interest

The authors have no conflicts to disclose.

Author Contributions

Tongshuai Zhu: Conceptualization (lead); Formal analysis (equal); Funding acquisition (lead); Investigation (lead); Methodology (lead); Visualization (lead); Writing – original draft (equal); Writing – review & editing (equal). **Hao Ni:** Software (supporting). **Dinghui Wang:** Formal analysis (equal); Writing – original draft (equal); Writing – review & editing (equal). **Zhilong Yang:** Formal analysis (equal); Writing – original draft (equal); Writing – review & editing (equal). **Guohui Zhan:** Formal analysis (equal); Writing – original draft (equal); Writing – review & editing (equal). **Baojun Wei:** Supervision (lead).

DATA AVAILABILITY

The data that support the findings of this study are available from the corresponding author upon reasonable request.

REFERENCES

[1]N. P. Armitage, E. J. Mele, and A. Vishwanath, "Weyl and Dirac semimetals in three-dimensional solids," Rev. Mod. Phys. **90**, 015001 (2018).
[2]S. M. Young, S. Zaheer, J. C. Teo, C. L. Kane, E. J. Mele, and A. M. Rappe, "Dirac semimetal in three dimensions," Phys. Rev. Lett. **108**, 140405 (2012).
[3]Z. Liu, B. Zhou, Y. Zhang, Z. Wang, H. Weng, D. Prabhakaran, S.-K. Mo, Z. Shen, Z. Fang, X. Dai *et al.*, "Discovery of a three-dimensional topological Dirac semimetal, Na_3Bi," Science **343**, 864–867 (2014).
[4]A. A. Burkov and L. Balents, "Weyl semimetal in a topological insulator multilayer," Phys. Rev. Lett. **107**, 127205 (2011).
[5]X. Wan, A. M. Turner, A. Vishwanath, and S. Y. Savrasov, "Topological semimetal and Fermi-arc surface states in the electronic structure of pyrochlore iridates," Phys. Rev. B **83**, 205101 (2011).
[6]T. M. McCormick, I. Kimchi, and N. Trivedi, "Minimal models for topological Weyl semimetals," Phys. Rev. B **95**, 075133 (2017).
[7]B. Yan and C. Felser, "Topological materials: Weyl semimetals," Annu. Rev. Condens. Matter Phys. **8**, 337–354 (2017).
[8]A. A. Burkov, M. D. Hook, and L. Balents, "Topological nodal semimetals," Phys. Rev. B **84**, 235126 (2011).
[9]C. Fang, H. Weng, X. Dai, and Z. Fang, "Topological nodal line semimetals," Chin. Phys. B **25**, 117106 (2016).
[10]C. Fang, Y. Chen, H.-Y. Kee, and L. Fu, "Topological nodal line semimetals with and without spin-orbital coupling," Phys. Rev. B **92**, 081201 (2015).
[11]Z.-M. Yu, Z. Zhang, G.-B. Liu, W. Wu, X.-P. Li, R.-W. Zhang, S. A. Yang, and Y. Yao, "Encyclopedia of emergent particles in three-dimensional crystals," Sci. Bull. **67**, 375–380 (2022).
[12]Z. Zhang, G.-B. Liu, Z.-M. Yu, S. A. Yang, and Y. Yao, "Encyclopedia of emergent particles in type-IV magnetic space groups," Phys. Rev. B **105**, 104426 (2022).
[13]G.-B. Liu, Z. Zhang, Z.-M. Yu, S. A. Yang, and Y. Yao, "Systematic investigation of emergent particles in type-III magnetic space groups," Phys. Rev. B **105**, 085117 (2022).
[14]L. Wu, F. Tang, and X. Wan, "Symmetry-enforced band nodes in 230 space groups," Phys. Rev. B **104**, 045107 (2021).
[15]F. Tang and X. Wan, "Complete classification of band nodal structures and massless excitations," Phys. Rev. B **105**, 155156 (2022).
[16]C. Fang, M. J. Gilbert, X. Dai, and B. A. Bernevig, "Multi-Weyl Topological Semimetals Stabilized by Point Group Symmetry," Phys. Rev. Lett. **108**, 266802 (2012).
[17]X. Huang, L. Zhao, Y. Long, P. Wang, D. Chen, Z. Yang, H. Liang, M. Xue, H. Weng, Z. Fang, X. Dai, and G. Chen, "Observation of the chiral-anomaly-induced negative magnetoresistance in 3D Weyl semimetal TaAs," Phys. Rev. X **5**, 031023 (2015).
[18]B. Q. Lv, H. M. Weng, B. B. Fu, X. P. Wang, H. Miao, J. Ma, P. Richard, X. C. Huang, L. X. Zhao, G. F. Chen, Z. Fang, X. Dai, T. Qian, and H. Ding, "Experimental discovery of Weyl semimetal TaAs," Phys. Rev. X **5**, 031013 (2015).
[19]L. Yang, Z. Liu, Y. Sun, H. Peng, H. Yang, T. Zhang, B. Zhou, Y. Zhang, Y. Guo, M. Rahn *et al.*, "Weyl semimetal phase in the non-centrosymmetric compound TaAs," Nat. Phys. **11**, 728–732 (2015).
[20]C.-L. Zhang, S.-Y. Xu, I. Belopolski, Z. Yuan, Z. Lin, B. Tong, G. Bian, N. Alidoust, C.-C. Lee, S.-M. Huang *et al.*, "Signatures of the Adler–Bell–Jackiw chiral anomaly in a Weyl fermion semimetal," Nat. Commun. **7**, 10735 (2016).
[21]G. Xu, H. Weng, Z. Wang, X. Dai, and Z. Fang, "Chern semimetal and the quantized anomalous Hall effect in $HgCr_2Se_4$," Phys. Rev. Lett. **107**, 186806 (2011).
[22]S.-M. Huang, S.-Y. Xu, I. Belopolski, C.-C. Lee, G. Chang, T.-R. Chang, B. Wang, N. Alidoust, G. Bian, M. Neupane, D. Sanchez, H. Zheng, H.-T. Jeng, A. Bansil, T. Neupert, H. Lin, and M. Z. Hasan, "New type of Weyl semimetal with quadratic double Weyl fermions," Proc. Natl. Acad. Sci. U. S. A. **113**, 1180–1185 (2016).
[23]G. Ding, J. Wang, Z.-M. Yu, Z. Zhang, W. Wang, and X. Wang, "Single pair of type-III Weyl points half-metals: $BaNiIO_6$ as an example," Phys. Rev. Mater. **7**, 014202 (2023).
[24]A. A. Zyuzin and A. A. Burkov, "Topological response in Weyl semimetals and the chiral anomaly," Phys. Rev. B **86**, 115133 (2012).
[25]D. T. Son and B. Z. Spivak, "Chiral anomaly and classical negative magnetoresistance of Weyl metals," Phys. Rev. B **88**, 104412 (2013).
[26]A. Burkov, "Chiral anomaly and transport in Weyl metals," J. Phys.: Condens. Matter **27**, 113201 (2015).
[27]K. Morishima and K. Kondo, "General formula of chiral anomaly for type-I and type-II Weyl semimetals," Appl. Phys. Lett. **119**, 131907 (2021).
[28]J. F. Steiner, A. V. Andreev, and D. A. Pesin, "Anomalous Hall effect in type-I Weyl metals," Phys. Rev. Lett. **119**, 036601 (2017).

[29]A. A. Burkov, "Anomalous Hall effect in Weyl metals," Phys. Rev. Lett. **113**, 187202 (2014).
[30]A. Bharti and G. Dixit, "Non-perturbative nonlinear optical responses in Weyl semimetals," Appl. Phys. Lett. **125**, 051104 (2024).
[31]L. Wu, S. Patankar, T. Morimoto, N. L. Nair, E. Thewalt, A. Little, J. G. Analytis, J. E. Moore, and J. Orenstein, "Giant anisotropic nonlinear optical response in transition metal monopnictide Weyl semimetals," Nat. Phys. **13**, 350–355 (2017).
[32]A. Bharti and G. Dixit, "Role of topological charges in the nonlinear optical response from Weyl semimetals," Phys. Rev. B **107**, 224308 (2023).
[33]J. Ma, Q. Gu, Y. Liu, J. Lai, P. Yu, X. Zhuo, Z. Liu, J.-H. Chen, J. Feng, and D. Sun, "Nonlinear photoresponse of type-II Weyl semimetals," Nat. Mater. **18**, 476–481 (2019).
[34]T. Morimoto, S. Zhong, J. Orenstein, and J. E. Moore, "Semiclassical theory of nonlinear magneto-optical responses with applications to topological Dirac/Weyl semimetals," Phys. Rev. B **94**, 245121 (2016).
[35]S. Patankar, L. Wu, B. Lu, M. Rai, J. D. Tran, T. Morimoto, D. E. Parker, A. G. Grushin, N. L. Nair, J. G. Analytis, J. E. Moore, J. Orenstein, and D. H. Torchinsky, "Resonance-enhanced optical nonlinearity in the Weyl semimetal TaAs," Phys. Rev. B **98**, 165113 (2018).
[36]C. Tzschaschel, J.-X. Qiu, X.-J. Gao, H.-C. Li, C. Guo, H.-Y. Yang, C.-P. Zhang, Y.-M. Xie, Y.-F. Liu, A. Gao *et al.*, "Nonlinear optical diode effect in a magnetic Weyl semimetal," Nat. Commun. **15**, 3017 (2024).
[37]Z. Ni, B. Xu, M.-Á. Sánchez-Martínez, Y. Zhang, K. Manna, C. Bernhard, J. Venderbos, F. De Juan, C. Felser, A. G. Grushin *et al.*, "Linear and nonlinear optical responses in the chiral multifold semimetal RhSi," npj Quantum Mater. **5**, 96 (2020).
[38]N. Nagaosa, T. Morimoto, and Y. Tokura, "Transport, magnetic and optical properties of Weyl materials," Nat. Rev. Mater. **5**, 621–636 (2020).
[39]H. Da, Q. Song, H. Ye, and X. Yan, "Nonreciprocal photonic spin Hall effect of magnetic Weyl semimetals," Appl. Phys. Lett. **119**, 081103 (2021).
[40]F. De Juan, A. G. Grushin, T. Morimoto, and J. E. Moore, "Quantized circular photogalvanic effect in Weyl semimetals," Nat. Commun. **8**, 15995 (2017).
[41]E. J. König, H.-Y. Xie, D. A. Pesin, and A. Levchenko, "Photogalvanic effect in Weyl semimetals," Phys. Rev. B **96**, 075123 (2017).
[42]F. Flicker, F. de Juan, B. Bradlyn, T. Morimoto, M. G. Vergniory, and A. G. Grushin, "Chiral optical response of multifold fermions," Phys. Rev. B **98**, 155145 (2018).
[43]B. Sadhukhan and T. Nag, "Role of time reversal symmetry and tilting in circular photogalvanic responses," Phys. Rev. B **103**, 144308 (2021).
[44]A. Pal, D. Varjas, and A. M. Cook, "Robust quantization of circular photogalvanic effect in multiplicative topological semimetals," Phys. Rev. B **110**, 155154 (2024).
[45]B. Sadhukhan and T. Nag, "Electronic structure and unconventional nonlinear response in double Weyl semimetal $SrSi_2$," Phys. Rev. B **104**, 245122 (2021).
[46]T. Nag and D. M. Kennes, "Distinct signatures of particle-hole symmetry breaking in transport coefficients for generic multi-Weyl semimetals," Phys. Rev. B **105**, 214307 (2022).
[47]Z.-H. Chen, Z.-Y. Fang, T.-X. Liu, H.-J. Duan, M. Yang, M.-X. Deng, and R.-Q. Wang, "Quantum oscillation of the circular photogalvanic effect in Weyl semimetals under strong magnetic fields," Phys. Rev. B **110**, 115149 (2024).
[48]C. Le and Y. Sun, "Topology and symmetry of circular photogalvanic effect in the chiral multifold semimetals: A review," J. Phys.: Condens. Matter **33**, 503003 (2021).
[49]Y. Zhang, J.-L. Wang, X.-L. Xue, Y. Nie, D.-N. Shi, S.-B. Zhang, L.-X. Chen, and L.-W. Shi, "Robust edge photogalvanic effect in thin-film WTe_2," Appl. Phys. Lett. **125**, 161101 (2024).
[50]K. Sun, S.-S. Sun, L.-L. Wei, C. Guo, H.-F. Tian, G.-F. Chen, H.-X. Yang, and J.-Q. Li, "Circular photogalvanic effect in the Weyl semimetal TaAs," Chin. Phys. Lett. **34**, 117203 (2017).
[51]M. Yamamoto, T. Nishijima, R. Ohshima, Y. Ando, and M. Shiraishi, "A circular photogalvanic effect in two-dimensional electron gas on the surface of $SrTiO_3$," Appl. Phys. Lett. **124**, 082401 (2024).
[52]H. B. Nielsen and M. Ninomiya, "Absence of neutrinos on a lattice: (I). Proof by homotopy theory," Nucl. Phys. B **185**, 20–40 (1981).
[53]H. B. Nielsen and M. Ninomiya, "Absence of neutrinos on a lattice: (II). Intuitive topological proof," Nucl. Phys. B **193**, 173–194 (1981b).
[54]Z. Zhang, Z.-M. Yu, G.-B. Liu, Z. Li, S. A. Yang, and Y. Yao, "MagneticKP: A package for quickly constructing $k\ p$ models of magnetic and non-magnetic crystals," Comput. Phys. Commun. **290**, 108784 (2023).
[55]X. Wang, F. Zhou, Z. Zhang, W. Wu, Z.-M. Yu, and S. A. Yang, "Single pair of multi-Weyl points in nonmagnetic crystals," Phys. Rev. B **106**, 195129 (2022).
[56]G. Kresse and J. Furthmüller, "Efficient iterative schemes for *ab initio* total-energy calculations using a plane-wave basis set," Phys. Rev. B **54**, 11169–11186 (1996).
[57]G. Kresse and D. Joubert, "From ultrasoft pseudopotentials to the projector augmented-wave method," Phys. Rev. B **59**, 1758–1775 (1999).
[58]J. P. Perdew, K. Burke, and M. Ernzerhof, "Generalized gradient approximation made simple," Phys. Rev. Lett. **77**, 3865–3868 (1996).
[59]P. E. Blöchl, "Projector augmented-wave method," Phys. Rev. B **50**, 17953–17979 (1994).
[60]G. Ding, J. Wang, H. Wu, W. Wang, D. Li, X.-P. Li, and X. Wang, "New recipe for enhancing the thermoelectric performance in topological materials carrying single-pair Weyl points fermions and phonons," Adv. Electron. Mater. **10**, 2300874 (2024).
[61]T. Zhu, H. Ni, B. Wei, and H. Wang, "Manipulating topological states in multi-Weyl semimetals by off-resonant light: Theory and material realization," Phys. Rev. B **110**, 235160 (2024).